

Suzaku Observations of the Centaurus Cluster: Absence of Bulk Motions in the Intracluster Medium

Naomi OTA,¹ Yasushi FUKAZAWA,² Andrew C. FABIAN,³ Takehiro KANEMARU,^{4,1}
Madoka KAWAHARADA,⁵ Naomi KAWANO,² Richard L. KELLEY,⁶ Takao KITAGUCHI,⁵
Kazuo MAKISHIMA,^{5,1} Kyoko MATSUSHITA,⁴ Kouichi MURASE,⁷ Kazuhiro NAKAZAWA,⁸
Takaya OHASHI,⁹ Jeremy S. SANDERS,³ Takayuki TAMURA,⁸ and Yuji URATA⁷

¹*Cosmic Radiation Laboratory, RIKEN, 2-1 Hirosawa, Wako, Saitama 351-0198*
ota@crab.riken.jp

²*Department of Physical Science, School of Science, Hiroshima University,*
1-3-1 Kagamiyama, Higashi-Hiroshima, Hiroshima 739-8526

³*Institute of Astronomy, Madingley Road, Cambridge CB3 0HA, UK*

⁴*Department of Physics, Tokyo University of Science, 1-3 Kagurazaka, Shinjuku-ku, Tokyo 162-8601*

⁵*Department of Physics, University of Tokyo, 7-3-1 Hongo, Bunkyo-ku, Tokyo 113-0033*

⁶*NASA/Goddard Space Flight Center, Code 662, Greenbelt, MD 20771, USA*

⁷*Department of Physics, Saitama University, Shimo-Okubo, Saitama 338-8570*

⁸*Institute of Space and Astronautical Science (ISAS/JAXA),*
3-1-1 Yoshinodai, Sagami-hara, Kanagawa 229-8510

⁹*Department of Physics, Tokyo Metropolitan University, 1-1 Minami-Osawa, Hachioji, Tokyo 192-0397*

(Received ; accepted)

Abstract

The Centaurus cluster ($z = 0.0104$) was observed with the X-ray Imaging Spectrometer (XIS) onboard the Suzaku X-ray satellite in three pointings, one centered on the cluster core and the other two offset by $\pm 8'$ in declination. To search for possible bulk motions of the intracluster medium, the central energy of He-like Fe-K line (at a rest-frame energy of 6.7 keV) was examined to look for a positional dependence. Over spatial scales of 50 kpc to 140 kpc around the cluster core, the central line energy was found to be constant within the calibration error of 15 eV. The 90% upper limit on the line-of-sight velocity difference is $|\Delta v| < 1400 \text{ km s}^{-1}$, giving a tighter constraint than previous measurements. The significant velocity gradients inferred from a previous Chandra study were not detected between two pairs of rectangular regions near the cluster core. These results suggest that the bulk velocity does not largely exceed the thermal velocity of the gas in the central region of the Centaurus cluster. The mean redshift of the intracluster medium was determined to be 0.0097, in agreement with the optical redshift of the cluster within the calibration uncertainty. Implications of the present results for the estimation of the cluster mass are briefly discussed.

Key words: galaxies: clusters: individual (The Centaurus cluster) — X-rays: galaxies — X-rays: ISM

1. Introduction

Clusters of galaxies are the most massive gravitationally bound structures in the Universe, and are thought to grow into larger systems through complex interactions between smaller systems. Signatures of such merging events may manifest themselves in non-Gaussian velocity distributions of member galaxies, temperature and density inhomogeneities in the intracluster medium (ICM), and bulk motions of the ICM. Indeed, numerical simulations predict the existence of bulk ICM flows with a substantial fraction of the virial velocity ($\sim 1000 \text{ km s}^{-1}$ for rich clusters), lasting several Gyr after each merger event (e.g., Roettiger et al. 1996; Norman & Bryan 1999). Therefore, measurements of the ICM velocity structure provide very important information with which to understand the cluster dynamics.

If the ICM has a significant bulk velocity compared to

its thermal velocity, the associated non-thermal pressure would endanger the assumption of hydrostatic ICM equilibrium, which is usually assumed in deriving the total gravitating mass in a cluster. For example, the factor 2–3 discrepancy between the X-ray and lensing mass estimations in some objects (e.g., Ota et al. 2004; Hattori et al. 1999) could be due to this effect. Therefore, the presence/absence of ICM bulk motion has a great impact on the cluster studies, including their mass estimates and cosmological applications.

We are thus encouraged to observationally constrain the ICM motion. Such an attempt may be carried out by examining X-ray emission lines from heavy elements for Doppler shifts and broadenings (e.g., Dupke & Bregman 2001), or by utilizing kinetic Sunyaev-Zel'dovich effects in the radio wavebands (e.g., Sunyaev et al. 2003). For the former method, X-ray spectroscopy of the emission lines from heavy ions, particularly the 6.7 keV K-lines

from Helium-like iron atoms, provides the most sensitive way of studying such ICM motions. By observing X-ray spectra in the 0.5–8.5 keV range from the core regions of the Centaurus cluster (Abell 3526) with the Chandra ACIS, Dupke & Bregman (2006) recently reported on a large velocity gradient of $2400 \pm 1000 \text{ km s}^{-1}$ over a spatial scale of 100 kpc, reconfirming their previous ASCA measurements (Dupke & Bregman 2001). However, their results might still be subject to residual uncertainties arising from temporal and intrachip gain variability, requiring an independent cross confirmation. Since a bulk velocity of 1000 km s^{-1} along the line of sight translates to a shift in the He-like Fe-K line energy of $\Delta E = 22 \text{ eV}$, we need not only sufficient photon statistics and good energy resolution, but also precise instrumental gain calibrations with an accuracy better than $\sim 20 \text{ eV}$ (or $\sim 0.3\%$).

The Centaurus cluster (Abell 3526), at the redshift of $z_{\text{cl}} = 0.0104$, is a nearby X-ray bright cluster of galaxies, hosting the cD galaxy NGC 4696. It has been extensively studied at various wavelengths. Lucey et al. (1986) found a bimodal velocity distribution of galaxies, corresponding to the main cluster (Cen 30) centered on NGC 4696, and a subcluster (Cen 45) centered on NGC 4709, with a velocity difference of $\sim 1500 \text{ km s}^{-1}$. They hence argued that Cen 30 is currently accreting Cen 45. The X-ray measured ICM temperature is $\sim 3.8 \text{ keV}$ in outer regions, and decreases toward the center to $\sim 1.7 \text{ keV}$ (e.g., Ikebe et al. 1999; Makishima et al. 2001; Takahashi et al. 2004). Although the central part of this cluster is relatively relaxed (e.g., Allen & Fabian 1994), at larger radii the temperature maps derived with ASCA reveal a hot spot coincident with Cen 45 (Churazov et al. 1999; Furusho et al. 2001), supporting the idea that there is a past or ongoing merger episode. The central region is very rich in metals, with a large abundance gradient (Fukazawa et al. 1994; Ikebe et al. 1999; Graham et al. 2006; Sanders & Fabian 2006). Emitting very intense Fe-K emission lines, the central region of the Centaurus cluster provides an excellent opportunity for a study of ICM bulk-motion.

In this paper, we present an analysis of the bulk velocity of the gas over the central 240 kpc of the Centaurus cluster, conducted with the X-ray Imaging Spectrometer (XIS; Koyama et al. 2006) on board the Suzaku satellite (Mitsuda et al. 2006). The XIS has an excellent sensitivity at the iron K-line energies, and a very low background. In addition, the current accuracy of the XIS in-orbit calibration is already high enough to enable us to make meaningful searches for possible ICM bulk motions. The Suzaku X-ray telescope (XRT; Serlemitsos et al. 2006) has a spatial resolution of $\sim 2'$ (Half Power Diameter; HPD), allowing us to study spatial velocity variations on reasonable scales (\sim a few arcminutes). We therefore test the previously claimed large velocity gradient near the cluster center.

Throughout this paper we adopt $\Omega_{\text{M}} = 0.3$, $\Omega_{\Lambda} = 0.7$, and $H_0 = 70 \text{ km s}^{-1} \text{ Mpc}^{-1}$; $1'$ corresponds to 13.5 kpc at the cluster redshift of $z_{\text{cl}} = 0.0104$. The quoted statistical errors refer to 68% confidence ranges, unless otherwise stated.

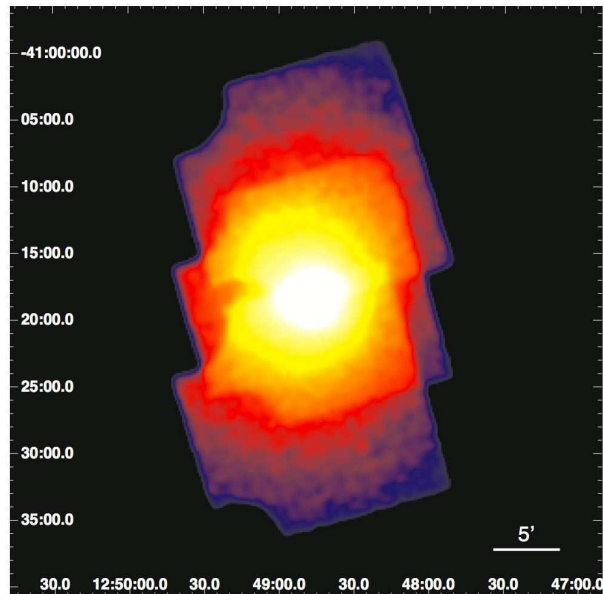


Fig. 1. Suzaku XIS0 smoothed image of the Centaurus cluster in the 0.4–10 keV band. The three pointing images are superimposed, but are not corrected for the overlapping exposure. Two corners of the CCD chip illuminated by the on-board calibration sources are excluded. The X-ray emission is peaked at NGC 4696. The subcluster centered on NGC 4709 is about $15'$ away from the center and outside the XIS fields of view.

2. Observation

Three pointed observations of the Centaurus cluster were conducted between 2005 December 27–29, in the Suzaku Phase-I period: one centered on the cD galaxy, NGC 4696, and the other two (Offset1 and Offset2) offset by $-8'$ and $+8'$ in declination, respectively. The details of the observations is given in table 1. The two on-board instruments, the XIS and the Hard X-ray Detector (HXD; Takahashi et al. 2006), were operated in their normal modes during the observations. The XIS consists of four X-ray sensitive CCD cameras: three front-illuminated (FI) CCDs and one back-illuminated (BI) CCD. In the present paper, we use data from the three FI-chip cameras (XIS0, 2, and 3), since they have higher sensitivities as well as lower backgrounds at the iron-K line energies, compared to the BI-chip camera (XIS1). As shown in figure 1, the extended ICM emission was clearly detected, the center of which $(\alpha, \delta) = (192^\circ.2058, -41^\circ.30424)$ in J2000 coordinates, is consistent within $\sim 25''$ of the position of NGC 4696.

The data reduction was performed using HEASOFT version 6.0.6. The XIS event lists created in the rev0.7 pipeline processing were filtered with the following criteria: the geomagnetic cut-off rigidity $> 6 \text{ GV}$, the elevation angle from the earth limb $> 10^\circ$, and the satellite outside the South Atlantic Anomaly. The net exposures are 29.4, 33.4, and 31.6 ks for the Center, Offset1, and Offset2 pointings, respectively. We selected XIS events

Table 1. Details of the Suzaku observations of the Centaurus cluster

Target name	Sequence No.	Date	Coordinates*		Roll angle (deg)	Exposure† (s)
			α (deg)	δ (deg)		
CENTAURUS_CLUSTER	800014010	2005 Dec 27	192.2054	-41.3111	-253.76	29397
CENCL_Offset1	800015010	2005 Dec 28	192.2054	-41.444	-253.72	33431
CENCL_Offset2	800016010	2005 Dec 29	192.2054	-41.178	-253.48	31647

* Pointing coordinates in J2000.

† Net exposure time of the XIS sensors after data filtering.

with grades 0, 2, 3, 4, and 6. The XIS response matrix files, `ae_xi[0,2,3]_20060213.rmf`, and the on-axis auxiliary files, `ae_xi[0,2,3]_xisnorm6_20060415.arf` were used in the spectral analysis.

3. Data analysis and Results

Our primary goal is to constrain the line-of-sight bulk velocity of the ICM using the iron-K line at 6.7 keV. For this purpose, the accuracy of photon energy measurements is crucial. We briefly review in §3.1 the current XIS calibration uncertainty, and describe in §3.2–§3.6 our analyses of the velocity structure of the ICM on small and large spatial scales.

3.1. Accuracy of the energy scale

In order to examine the accuracy of the XIS energy scale, we checked the following three key points: the line centroid energies of calibration sources illuminating some corners of the CCD chips, the positional gain variations due to Charge Transfer Inefficiency, and the agreement of line centroid energies among the three pointings onto the same sky regions of the Centaurus cluster.

The fiducial absolute energy scale of the XIS is provided by Mn-K α lines from the built-in calibration sources (^{55}Fe), which illuminates two out of four corners of each XIS chip. For the three pointings, we fitted these lines with a Gaussian, and confirmed that the obtained line centroids of XIS0, XIS2, and XIS3 all agree within 0.02–0.1% of the expected value of 5.8951 keV.

Although the calibration isotope fixes the fiducial energy scale, the gain could vary from place to place on the same CCD chip (intrachip gain variation), due to Charge Transfer Inefficiency (CTI). The CTI increases with time due to irradiation by charged particles, enhancing the intrachip gain variations particularly along the direction of charge transfer (so called ACT-Y axis). The CTI characteristics of the XIS were calibrated in orbit using two line-rich extended sources, the Cygnus Loop and Sgr C, observed on 2005 November 23–24 and 2006 February 20–23, respectively. As a result, the gains of the four XIS sensors have been equalized over the CCD chips to an accuracy of $\pm 0.2\%$ (Koyama et al. 2006). These results have been used to produce the rev0.7 data. As the three observations of the Centaurus cluster were carried out on successive days between those of the Cygnus Loop and Sgr C, our analysis should be little affected by any temporal gain variation.

We further examined the rev0.7 data of two other extended sources, Abell 1060 and Abell 426, observed on 2005 November 22 and 2006 February 1, respectively. The ACT-Y dependence of the iron line energy was then confirmed to be very small, typically within $\pm 0.2\%$. From these calibrations, we consider that the intrachip gain variations of the rev0.7 data from the four XIS sensors are at most $\pm 0.2\%$ (± 15 eV) in the ACT-Y direction. The gain variation along the ACT-X axis is also within $\pm 0.2\%$, as confirmed with Sgr C, Abell 1060, and Abell 426. Quantitative confidence levels of the systematic error were estimated based on a detailed analysis of Abell 426, which has the most intense iron-K lines among the celestial calibrators utilized here. Since the four XIS sensors are placed on the focal plane in different orientations with respect to the satellite coordinate (Koyama et al. 2006), the positional gain variation is effectively studied by comparing the line energies of the same sky regions (namely different detector regions) on the four sensors. We thus divided the XIS field of view of the Abell 426 observation into 8×8 cells of size $2'.1 \times 2'.1$, and estimated the 1σ systematic error on the iron line energy by calculating the chi-square value, defined as $\chi^2 = \sum_{\text{cell}} \sum_{i=0}^3 (E_i - \langle E \rangle)^2 / (\sigma_i^2 + \sigma_{\text{sys}}^2)$. Here E_i and σ_i are the iron-K line centroid energy and the 1σ statistical error obtained with XIS- i in a certain cell, respectively, $\langle E \rangle = \sum_{i=0}^3 E_i / 4$ is the mean iron-K energy, and \sum_{cell} sums up all cells. If a systematic error of $\sigma_{\text{sys}} = 10$ eV (i.e., $\pm 0.13\%$) is tentatively employed, we obtain $\chi^2/\nu = 1.1$ for 144 degrees of freedom. This value of σ_{sys} is hence considered appropriate as a measure of the residual gain non-uniformity.

Utilizing the overlaps between the three pointings of the Centaurus cluster (figure 1), we examined whether the central line energy of the same sky region turns out to be the same when measured in the different pointings (and hence by different regions on the CCD chip). In detail, we derived the iron-line energy of the central pointing data of the three FI chips from a $8'.5 \times 15'$ region (roughly coincident with southern half of the XIS field of view in the central pointing), and compared it with that of the same sky region observed in Offset1. The results agree with each other within 0.1%. Similarly, the Fe-K line energy averaged over a northern $8'.5 \times 15'$ region showed a good agreement (0.1%) between the central pointing and Offset2. If we divide a central $8'.5 \times 8'.5$ square region centered on the cD galaxy into 4×4 cells of size $2'.1 \times 2'.1$ each, the energy scales are again in good agreement between the central pointing and the two offsets; $\lesssim 0.2\%$ in

14 cells, and $\lesssim 0.3\%$ in 2 cells (with 1σ statistical errors being ~ 20 eV).

Based on these examinations, we decided to take $\pm 0.13\%$ ($\pm 0.2\%$) as the systematic error on the XIS energy scale at the 68% (90%) confidence level. The 68% systematic error corresponds to ± 10 eV in terms of the iron-K line energy, or ± 0.0015 in redshift, or ± 470 km s^{-1} in line-of-sight velocity.

3.2. Analysis of small-scale velocity structure

Now that we have confirmed the XIS energy-scale is accurate, we proceed to the study of the velocity structure of the ICM in the Centaurus cluster on a scale of a few arcminutes. For this purpose, we divided the $18' \times 18'$ square XIS field of view into 8×8 cells as shown in figure 2. Thus, each cell covers a sky area of $2'.1 \times 2'.1$ ($=28$ kpc $\times 28$ kpc). Since the energy scale is consistent among the three XIS sensors and among the three pointings (§3.1), we co-added the data from XIS0, XIS2, and XIS3, and merged the three pointings where they overlap. Excluding the calibration source regions, 52 cells in total were used in the spectral fitting. The composite spectra were rebinned so that each spectral bin had more than 30 counts.

Figure 3 shows an example of the XIS spectrum obtained in this way, displayed over the iron energy band. Thus, we observe a very intense He-like Fe-K α line, a weaker H-like Fe-K α line, and a blend between He-like Ni-K α and He-like Fe-K β lines. In the 5–10 keV band, the source count rate measured in each cell ranges from 1.6×10^{-3} to 2.5×10^{-2} c s^{-1} per XIS sensor, with a mean over the 52 cells being 6.9×10^{-3} c s^{-1} . If the energy band is limited to 6.5–6.9 keV, in which the He-like Fe K α line emission is prominent, these count rates decrease by a factor of 3–5.

Background spectra were derived by integrating events over the same regions on the detector planes as the on-source data integration, using a blank-sky observation towards the North Ecliptic Pole conducted on 2005 September 2–4 for 95 ks. At the cluster center, the background surface brightness in the 5–10 keV range is only a few percent of that of the ICM emission, while the background contribution increases to ~ 35 percent near the edge of the XIS field of view. The XIS background spectrum has several instrumental fluorescent lines in the energy band of interest, with the most prominent one being Ni-K α line at 7.48 keV. However, as shown in figure 3, the background spectrum can be regarded as featureless in the energy range where the He-like Fe-K α line from the Centaurus cluster is present. We subtracted the backgrounds from the on-source spectra, and confirmed that this process does not change the Fe-K line energy.

3.3. Modeling the iron-K lines

To accurately determine the iron-line energies, we fitted the background-subtracted XIS spectra with a simple model over the 5 – 10 keV energy range. The model we chose consists of a continuum represented by the APEC thermal emission model with metal abundances reset to zero ($Z = 0$), and three Gaussians for the major line com-

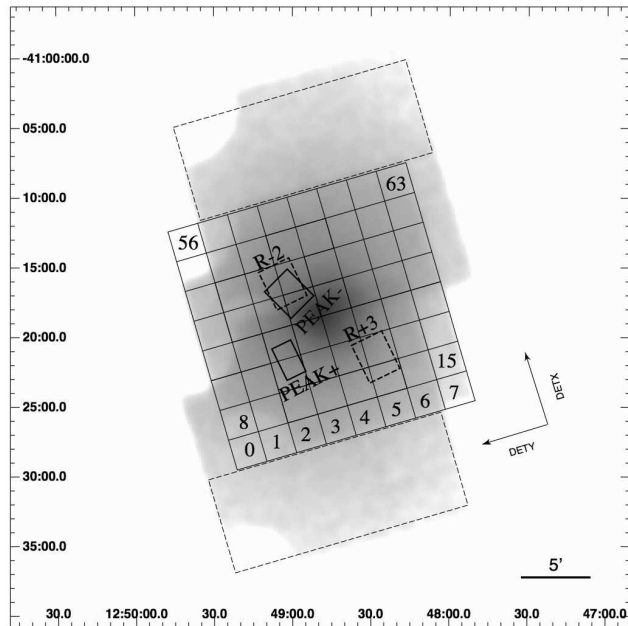


Fig. 2. An image showing the spectral accumulation regions. The central 8×8 cells, each with a size of $2'.1 \times 2'.1$, are designated as #0 \sim #63, and were used for the study of small-scale velocity structure. The two larger rectangular regions (the dashed boxes of size $7' \times 18'$) were used for the larger-scale analysis. The four regions used for comparison with the Chandra results (Dupke & Bregman 2006) are also shown as PEAK-, PEAK+ (the solid boxes), R-2, and R+3 (the dashed boxes).

ponents: the He-like Fe-K α line at 6.70 keV, the H-like Fe-K α line at 6.97 keV, and a 7.83 keV line representing the blend of He-like Ni-K α line (7.80 keV) and He-like Fe-K β line (7.90 keV). The quoted line energies refer to their rest-frame values.

The He-like Fe-K α complex, consisting of 26 lines, exhibits an asymmetric shape (e.g., Dubau & Volonte 1980). Although the line profile becomes essentially Gaussian when convolved with the XIS energy resolution [~ 160 eV (FWHM) at the time of the observations of the Centaurus cluster; Koyama et al. 2006], the Gaussian centroid energy, denoted E_0 , can no longer be identified with that of the strongest component, namely the resonance line at 6.6986 keV in the rest frame. To determine the expected value of E_0 when the ICM has no bulk motion and the cluster is at zero redshift, we produced a simulated spectrum employing the APEC model and XIS energy response. Based on ASCA measurements (Furusho et al. 2001; Ikebe et al. 1999), the simulation assumed an ICM temperature of $kT \sim 3$ keV, and a metallicity of $Z = 1Z_{\odot}$. By fitting the simulated spectrum with an APEC plus three Gaussian model as described above, we obtained $E_0 = 6.6771 \pm 0.0001$ keV. We thus assume the rest-frame He-like Fe-K α centroid energy to be $E_0 = 6.677$ keV.

Strictly speaking, the value of E_0 is expected to depend upon the ICM temperature; as the temperature decreases, contributions from lower-ionization ions increase, making

E_0 shift towards lower energies. For example, the shift is by about 1% when $kT = 1$ keV. The very center of the Centaurus cluster is known to host a cool component with a temperature of $kT \sim 1.7$ keV (Ikebe et al. 1999; Sanders & Fabian 2002; Takahashi et al. 2004). However, the effect of the cool plasma on the line-centroid measurement is estimated to be negligible, because the cool gas is localized within $1'$ from the cD galaxy with a relatively minor emission integral (Ikebe et al. 1999; Sanders & Fabian 2002; Takahashi et al. 2004), and the Fe-K line emissivity of the 1.7 keV gas is by more than a factor of 2 (7) lower than that of > 2 keV (> 3 keV) gas. Towards higher temperatures, E_0 can be regarded as constant within 0.1% as long as $2 \text{ keV} < kT < 8 \text{ keV}$.

The intrinsic line width of the He-like Fe-K α complex emitted from the 3 keV gas is derived to be $\sigma_0 = 27.8 \pm 0.2$ eV. This is smaller than the instrumental energy resolution at ~ 7 keV, ~ 70 eV in Gaussian sigma, and hence a minor contributor to the observed total line width. The possibility of the line broadening in excess of the intrinsic width is discussed in §4.3.

3.4. Result of spectral fitting

Using XSPEC version 11, we fitted the 5–10 keV spectra from individual cells with the APEC plus three Gaussian line model described in §3.3. The three Gaussian energies were allowed to vary, but their relative energies were constrained to obey their rest-frame ratios. Since the XIS energy resolution δE depends on energy E approximately as $\delta E \propto E^{0.5}$ in the energy band of interest, and varies gradually with time (Koyama et al. 2006), the Gaussian widths were included as free parameters, with their relative values constrained to scale with the square root of the line energies. The normalizations of the APEC and three Gaussians were also left free. Although the analysis utilizes the χ^2 fitting method, consistent results are derived if unbinned spectra are fitted by the maximum likelihood method.

An example of the spectral fit is shown in figure 3. We obtained an acceptable fit at the 90% confidence level from 49 out of the 52 cells (except # 2, 22, and 33), and at the 95% level from all the cells. The reduced χ^2 values, χ^2_ν , range from 0.68 to 1.53 in the central 6×6 cells, where the number of degrees of freedom ν ranges from 15 to 132. In the outer 19 cells, χ^2_ν is between 0.30 and 1.85, and ν between 3 and 27. The value of ν varies as the number of spectral bins changes, due to the spectral binning criterion.

The line centroids have been constrained in most cases, with the 1σ statistical errors of $\sigma_{\text{fit}} = 3 - 4$ eV for the inner 2×2 cells, $\sim 4 - 8$ eV for the surrounding 12 cells, and ~ 10 eV for outer 17 cells surrounding the central 4×4 cells. In most of these 33 cells, the fitted Gaussian widths are consistent, within the 90% statistical errors, with those found with the Mn-K α calibration line ($\sigma_{\text{inst}} \sim 40$ eV). On the other hand, those cells lying near the edge of the field of view have too poor photon statistics to constrain the line width. In analyzing the outermost 19 cells, we thus fixed the line width at 40 eV and the ICM temperature

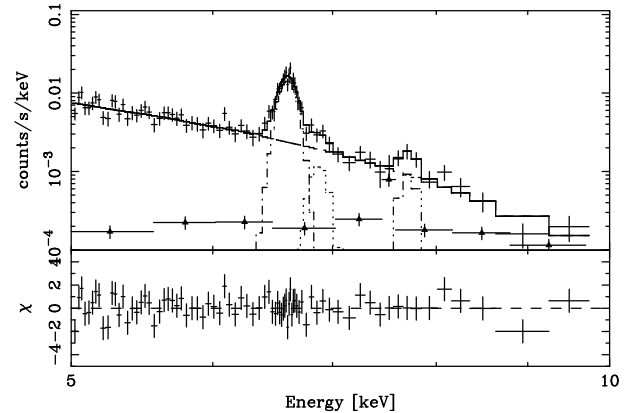


Fig. 3. Background-subtracted XIS0+XIS2+XIS3 spectrum of cell #44 in the 5–10 keV band (the crosses), fitted with the APEC model with $Z = 0$ for the continuum (the dashed line) and three gaussian lines; the dash-dot line for the He-like K α , the dotted line for H-like K α , and the dash-dot-dot line for a blend of He-like Ni K α and He-like Fe K β . The best-fit total model is shown with the solid line. The background spectrum taken from the North Ecliptic Pole observation is also shown (the crosses with triangle). The bottom panel shows the residuals of the fit in terms of the ratio of the residual to the uncertainty of each measurement, which is also the contribution to χ^2 when squared.

at 3.0 keV.

The fitted line centroids, E_{obs} , are then converted to redshifts through $z = (E_0 - E_{\text{obs}})/E_{\text{obs}}$ using $E_0 = 6.677$ keV. The obtained results are plotted in figure 4, where the implied ICM radial velocity, $v_r \equiv c(z - z_{\text{cl}})$, is also indicated on the right-side ordinate of the panels. As seen from this plot, the measured redshifts are consistent, in almost all the 52 cells, with the optical value within the current 90% calibration errors (± 0.002 in terms of redshift).

The weighted mean (and the standard deviation) of the line centroid measured in the 52 cells is $\langle E_{\text{obs}} \rangle = 6.6133$ keV (± 0.0162 keV). The reduced chi-square around this mean is $\chi^2_\nu = \nu^{-1} \sum ((E_{\text{obs}} - \langle E_{\text{obs}} \rangle) / \sigma_{\text{fit}})^2 = 1.1$ with $\nu = 51$. Thus the measured E_{obs} values are consistent with being constant at the 90% confidence level. The mean redshift (and the standard deviation) of the ICM is determined to be $\langle z_{\text{obs}} \rangle = 0.0097$ (± 0.0024), which agrees with the optical redshift of the cluster $z_{\text{cl}} = 0.0104$ within the calibrational uncertainty. For reference, the optical redshift of the cD galaxy is $z_{\text{cD}} = 0.009867$ (the NED database). The difference between z_{cD} and z_{cl} , 0.0005, however, is not distinguishable given the present accuracy of the energy scale.

3.5. Other systematic errors

The Point Spread Function (PSF) of the Suzaku X-ray telescopes has a width of $\sim 2'$ (in half-power diameter), which is comparable to the size of the spectral regions examined here. This means that photons we detect in a certain spectral accumulation region are the sum of those coming from the corresponding sky region, C_1 , and those from its surroundings, C_2 . We estimated this effect by

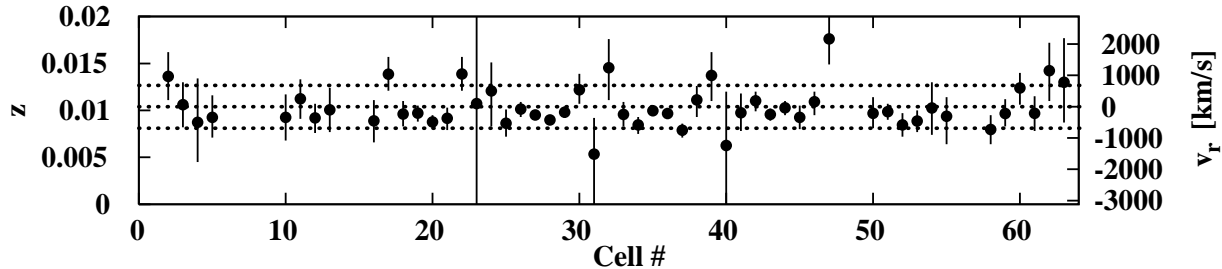


Fig. 4. Results of the redshift measurements using the He-like Fe-K lines in 52 cells. The left and right axes show the redshift and radial velocity of the ICM, respectively. See figure 2 for the definitions of the spectral regions. The error bars are 1σ statistical. The optical redshift of $z_{c1} = 0.0104$ and the range of the present calibration error at the 90% confidence level, ± 0.002 in redshift (or ± 700 kms^{-1} in the line-of-sight velocity), are indicated with the horizontal dotted lines.

the *xissim* ray-tracing simulator (Ishisaki et al. 2006), assuming a $kT = 3$ keV APEC model for the spectral distribution and a double β model for the surface brightness distribution. According to Mohr et al. (1999), the two β components are assumed to have core radii of $r_{c1} = 99$ kpc and $r_{c2} = 8.6$ kpc, the same slope parameter $\beta = 0.569$, and a surface brightness ratio of $I_2/I_1 = 43$ at the center. This simulation yielded $C_1 : C_2 \sim 0.4 : 0.6$ in cells lying at $r < 4'.5$ from the center, and $C_1 : C_2 \sim 0.5 : 0.5$ in cells surrounding them. Therefore, the results in figure 4 remains valid, as long as the spatial resolution of the analysis is regarded as $\sim 4'$ (~ 50 kpc) instead of $\sim 2'$.

As reported in Serlemitsos et al. (2006), the attitude of Suzaku sometimes drifts in both DETX/Y directions with a typical peak-to-peak amplitude about $0'.5 - 1'$, mainly synchronized with the spacecraft orbital period (96 min). This effect blurs the spatial photon distribution on the detector plane, because the size of the spectral accumulation regions is relatively small ($\sim 2'$) in our analysis. To examine this issue, we performed Lorentzian fitting to central X-ray surface brightness profiles projected onto the DETX or DETY axis, and determined the X-ray centroid position of the cluster every 256 seconds, without relying on the attitude solution. As a result, the amplitudes of the drift were found to be small in this particular observation: $\Delta\text{DETX} \sim 37''$ and $\Delta\text{DETY} \sim 43''$. We produced a mock attitude file (that describes temporal change of the satellite's euler angles) assuming that the cluster centroid position moves sinusoidally with a peak-to-peak amplitude of $40''$ in the DETX/Y directions and the 96-min period. By repeating the same ray-tracing simulation incorporating this mock attitude file, the effect of the attitude drift on the photon counts (C_1 or C_2) was estimated to be $\lesssim 10\%$, and typically $C_1 : C_2 \sim 0.4 : 0.6$ inside the XIS field of view. Therefore the effect of attitude drift is negligible compared to the original PSF effects.

3.6. Analysis of larger-scale velocity structure

In order to search the X-ray data for larger-scale velocity gradients in the ICM, we compared the redshift in the following three regions; the central $18' \times 18'$ square, and two $7' \times 18'$ rectangular regions which are offset northwards/southwards by about $12'$ (two dashed boxes in figure 2). The spectral fits in the 5–10 keV band yield

$z = 0.00993 \pm 0.00015 (\pm 0.0015)$, $0.0119 \pm 0.0011 (\pm 0.0015)$, and $0.0094 \pm 0.0015 (\pm 0.0015)$, for the central, northern offset, and southern offset regions, respectively. The 68% statistical errors and (the 68% systematic errors) are quoted. The radial velocity is then $v_r = -144 \pm 44 (\pm 470)$ kms^{-1} , $441 \pm 316 (\pm 470)$ kms^{-1} , and $-306 \pm 450 (\pm 470)$ kms^{-1} for the three regions, respectively. Thus, no significant velocity variation on ~ 10 -arcminutes scales is seen from the above analysis. Taking the sum of the statistical and systematic errors in quadrature, we estimate the 90% upper limit on the velocity gradient among the above three regions to be $|\Delta v| < 1400$ kms^{-1} .

4. Discussion

From the careful analysis of the high-quality Fe-K line data obtained with the Suzaku XIS, we found no evidence of significant spatial gradients in the Fe-K line center energies inside the XIS fields of view. The derived upper limits apparently exclude the large velocity difference previously claimed by Dupke & Bregman (2006). In §4.1, we further investigate this issue by analyzing the same regions as studied by Dupke & Bregman (2006). In §4.2, implications of the present results are discussed, followed by §4.3 where we constrain Doppler broadening of the Fe-K lines in search for turbulent motions of the ICM.

4.1. Comparisons with previous results

A large velocity difference by ~ 2500 kms^{-1} was reported in the core of the Centaurus cluster based on the previous ASCA and Chandra observations (Dupke & Bregman 2001; Dupke & Bregman 2005; Dupke & Bregman 2006). Specifically, by comparing the redshifts measured with the Chandra/ACIS-S3 spectra in various regions near the cluster center, Dupke & Bregman (2006) obtained (1) a maximum velocity gradient of $\Delta v = 2900 \pm 700$ kms^{-1} between a pair of rectangular regions, $2'.3 \times 2'.7$ (PEAK-) and $1'.5 \times 2'.5$ (PEAK+), and (2) another large difference by $\Delta v = 2400 \pm 1000$ kms^{-1} between two $2'.4 \times 3'$ regions (R-2 and R+3). We show these four regions on our figure 2.

Since the report by Dupke & Bregman (2006) apparently disagrees with our results, we examined the present Suzaku data for the above two cases, by accumulating

spectra from the same sky regions on the three FI chips. (As seen in figure 2, the PEAK- and PEAK+ regions are located near cells #35 and #18, and R-2 and R+3 are near cells #43 and #21 in our analysis.) After co-adding the central and offset data, the total exposure time is 183 ks for PEAK- and R-2, and 188 ks for PEAK+ and R+3; these are about 5 times longer than the Chandra exposure.

As to (1), the model fitting to the XIS spectra has given $z_- = 0.0101 \pm 0.0005 (\pm 0.0015)$, and $z_+ = 0.0079 \pm 0.0012 (\pm 0.0015)$, resulting in a negative value for the redshift difference $\Delta z \equiv z_+ - z_- = -0.0022 \pm 0.0013 (\pm 0.0022)$, or the velocity difference, $\Delta v = c\Delta z = -660 \pm 390 (\pm 660) \text{ km s}^{-1}$. Because PEAK- and PEAK+ are close to each other, the intrachip gain difference between them is considered to be smaller than our canonical value, $\pm 470 \text{ km s}^{-1}$. Nevertheless, to be conservative, we multiplied this by $\sqrt{2}$, to obtain $\pm 660 \text{ km s}^{-1}$ as our systematic error on the velocity difference. The above results then imply that the velocity difference between PEAK- and PEAK+ does not significantly exceed the calibration uncertainty of $\pm 660 \text{ km s}^{-1}$. If we further sum the systematic and statistical errors in quadrature, the 90% confidence range becomes $-1890 \text{ km s}^{-1} < \Delta v < +570 \text{ km s}^{-1}$, which is inconsistent with the Chandra measurement of $2900 \pm 700 \text{ km s}^{-1}$. The results are summarized in table 2.

As to (2), a similar analysis of the Suzaku XIS data has given the redshifts of the R-2 and R+3 regions as $z_{R-2} = 0.0107 \pm 0.0006 (\pm 0.0015)$ and $z_{R+3} = 0.0089 \pm 0.0010 (\pm 0.0015)$, respectively. Therefore, the redshift and velocity differences become $\Delta z = z_{R+3} - z_{R-2} = -0.0018 \pm 0.0012 (\pm 0.0022)$ and $\Delta v = -540 \pm 360 (\pm 660) \text{ km s}^{-1}$, respectively (table 2). The allowed 90% range then becomes $-1730 \text{ km s}^{-1} < \Delta v < +650 \text{ km s}^{-1}$, which again excludes the Chandra measurement of Δv between R-2 and R+3.

Then, can we reconcile the apparently conflicting Chandra (plus ASCA) and Suzaku results? One possibility is that the much wider PSF of the Suzaku XRT, compared to that of Chandra, has diluted the velocity gradient. To examine the effect, we again executed the `xissim` simulation of the XIS spectra for PEAK- and PEAK+, simply assuming that the gas bulk motion exists only in those two regions and that they have the velocity difference close to the 90% lower limit of the Chandra result, $\Delta v = +1700 \text{ km s}^{-1}$; other regions in the XIS field of view are assumed to have no bulk motion, with $z = 0.0104$. The model fit to the two simulated spectra indicates that the Suzaku XIS should observe a velocity difference of $\Delta v = +690 \text{ km s}^{-1}$, as a result of the telescope resolution which reduce the velocity difference by a factor of ~ 2.5 . Therefore, the Chandra measurement may be brought to be marginally consistent with the present Suzaku upper limit. As to (2), the same simulation indicates that the 90% lower-limit value of $\Delta v = +760 \text{ km s}^{-1}$ between R-2 and R+3 based on the Chandra report will be reduced to $\Delta v = +300 \text{ km s}^{-1}$ in the XIS data after smeared by the PSF. This is consistent with the 90% upper limit set by Suzaku, $+650 \text{ km s}^{-1}$.

In this way, the positive Δv reported by Dupke &

Bregman (2006) for the two pairs of regions can be tentatively made consistent with the negative Δv we measured. However, this was possible by invoking rather extreme assumptions; namely, to employ the Chandra lower limit and the Suzaku upper limit on Δv , and to assume that the ICM bulk motion is localized to the small regions of $\sim 25 \text{ kpc}$.

A comparison of the present results with the reported ASCA measurement (Dupke & Bregman 2001) may give additional clues. The Suzaku XRT (Serlemitsos et al. 2006) is an improved version over its predecessor onboard ASCA. Similarly, the Suzaku XIS is an improved instrument based on the SIS experiment onboard ASCA. As compared with the XRT+SIS combination onboard ASCA, the XRT+XIS of Suzaku hence has a ~ 1.5 times better PSF, a ~ 4.5 times larger effective area (at 7 keV; two SIS sensors versus three XIS cameras). Furthermore, the energy scale of the Suzaku XIS has been better calibrated (Koyama et al. 2006) than the ASCA SIS which was the first single-photon detection CCD used in cosmic X-ray observations. Therefore, any Doppler shifts in the Fe-K line detectable by ASCA would be detected by Suzaku with a much higher significance (unless the exposure is too short).

From these considerations, we conclude that it is rather difficult to reconcile the the present results with the Chandra (plus ASCA) measurements. Additional information will be obtained by analyzing a longer Chandra dataset on the Centaurus cluster. (Fabian et al. 2005).¹

4.2. Implications of the derived upper limits

Utilizing the Fe-K α line, we obtained a 90% upper limit on the velocity difference of $|\Delta v| < 1400 \text{ km s}^{-1}$ between any pair of regions within the XIS field of view, separated typically by $\sim 50 \text{ kpc}$ or more. This gives a tighter constraint on the ICM bulk motion than was suggested by previous reports. Since the ion sound velocity in the ICM is $s \equiv (\gamma P/\rho)^{1/2} = (\gamma kT/\mu m_p)^{1/2} \sim 880 \text{ km s}^{-1}$ for a temperature of $kT = 3 \text{ keV}$, our results imply that the line-of-sight velocity of the ICM bulk motion, if any, does not largely exceed the sound velocity. In other words, the ram pressure associated with the ICM bulk motion is at most comparable to the thermal ICM pressure, thus approximately validating the assumption of hydrostatic equilibrium in calculating the cluster mass. Of course, we can probe the gas motion only along the line of sight, and hence we need to assume 3-dimensional velocity structures in order to quantitatively utilize the present upper limits.

As an elementary exercise, below we evaluate the upper limit on rotational motion assuming for simplicity that the gas is rigidly rotating at a typical circular velocity of $\sigma_r \sim |\Delta v|/2$, and derive its quantitative effect on cluster mass estimation. Assuming an approximate spherical symmetry, and including the centrifugal force, the balance against the gravitational pull at a radius r on the rotational equatorial plane then becomes

¹ Some of the present authors actually analyzed this data set, but did not detect any significant velocity differences between the R-2 and R+3 regions identified by Dupke & Bregman (2006).

Table 2. Comparisons of velocity differences measured with Suzaku and Chandra

Region	Suzaku/XIS	Chandra/ACIS
	Δv (kms ⁻¹)*	Δv (kms ⁻¹) [†]
PEAK-, PEAK+	$-660 \pm 390 (\pm 660)$	2900 ± 700
R-2, R+3	$-540 \pm 360 (\pm 660)$	2400 ± 1000

* The velocity difference derived from the XIS spectra. The 68% statistical errors and (the 68% systematic errors) are quoted. [†] The velocity difference and the 1σ error derived from the Chandra ACIS spectra (Dupke & Bregman 2006).

$$-\frac{GM(r)\rho_{\text{gas}}}{r^2} = \frac{\partial P_{\text{gas}}}{\partial r} - \frac{f\rho_{\text{gas}}\sigma_r^2}{r}, \quad (1)$$

where $M(r)$ is the cluster mass interior to radius r , ρ_{gas} is the gas density, $P_{\text{gas}} = \rho_{\text{gas}}kT(\mu m_p)^{-1}$ is the ICM pressure, and f is the fraction of the ICM that is rotating ($0 \leq f \leq 1$). The gas density profile of the Centaurus cluster roughly follows $\rho_{\text{gas}} \propto r^{-1}$ within the central $r \lesssim 10'$ region, assuming the double- β model (Ikebe et al. 1999; Mohr et al. 1999). Together with the assumption $\sigma_r \propto r$, this yields

$$f\rho_{\text{gas}}\sigma_r^2 \propto r, \quad (2)$$

and hence the second term on the right-hand side of equation 1 can be rewritten as

$$\frac{f\rho_{\text{gas}}\sigma_r^2}{r} = \frac{\partial(f\rho_{\text{gas}}\sigma_r^2)}{\partial r}. \quad (3)$$

Equation 1 then becomes

$$\begin{aligned} -\frac{GM(r)}{r^2} &= \frac{1}{\rho_{\text{gas}}} \frac{\partial P_{\text{gas}}}{\partial r} + \frac{1}{\rho_{\text{gas}}} \frac{\partial(f\rho_{\text{gas}}\sigma_r^2)}{\partial r} \\ &= \frac{1}{\rho_{\text{gas}}} \frac{\partial}{\partial r} P_{\text{gas}}(1 + f\beta_r), \end{aligned} \quad (4)$$

where

$$\beta_r \equiv \frac{\mu m_p \sigma_r^2}{kT} \sim 1.07 \left(\frac{\mu}{0.63} \right) \left(\frac{\sigma_r}{700 \text{ kms}^{-1}} \right)^2 \left(\frac{kT}{3 \text{ keV}} \right)^{-1} \quad (5)$$

is the ratio of the kinetic energy due to rotational motion to the thermal energy. Thus, the total mass should be higher than the hydrostatic mass by a factor of $(1 + f\beta_r)$, because of the presence of additional pressure support.

At a typical radius of ~ 100 kpc, the rotational velocity is $\sigma_r < |\Delta v|/2 = 700 \text{ kms}^{-1}$, yielding $(1 + f\beta_r) \lesssim 2$. Considering an inclination angle i of the rotation axis and the mean $\sin i$ factor, $2/\pi$, the rotational velocity is $\sigma_r < |\Delta v|/2 \sin i = 1100 \text{ kms}^{-1}$ and $(1 + f\beta_r) \lesssim 3.6$. Therefore cluster mass estimation with the assumption of hydrostatic equilibrium is justified within a factor of $\sim 2 - 3.6$. In order to put a stronger constraint on the cluster mass to compare with other techniques (particularly gravitational lensing), a two-fold improvement on the energy-scale calibration is necessary.

4.3. Turbulent broadening of iron lines

The velocity structure in the cluster can also be studied by analyzing the X-ray line widths for turbulent Doppler broadening of the X-ray emission lines. The iron ions provide the best tracers of this effect, because the broadening due to a turbulent velocity, σ_{turb} , on the order of $\sim 300 \text{ kms}^{-1}$, can exceed their thermal broadening

($\sim 2 \text{ eV}$) by several times (Inogamov & Sunyaev 2003). However, considering the energy resolution of the FI CCDs, 160 eV (FWHM) or 70 eV (Gaussian 1σ), what can be done with the present data is at most to examine the observed Fe-K line width for possible broadening beyond the instrumental energy resolution and its intrinsic line width ($\sigma_0 \sim 28 \text{ eV}$ for $kT = 3 \text{ keV}$). In order to carry out this search under the highest statistics, we again fitted the XIS0+XIS2+XIS3 spectrum from the central $18' \times 18'$ region (analyzed in §3.6) with the APEC plus three Gaussian model. Here we assumed that the gas has no bulk velocity, and fixed the centroid of the He-like K α line to $6.677(1 + z_{\text{cl}})^{-1} \text{ keV}$. As a result, the Gaussian width has been obtained as $\sigma = 47 \pm 2 \text{ eV}$.

Since the degradation of the energy resolution with time is not currently implemented in the XIS response matrix (Koyama et al. 2006), the fitted Gaussian width is expressed by $\sigma^2 = \sigma_{\text{inst}}^2 + \sigma_0^2 + \sigma_{\text{turb}}^2$, where σ_{inst} is the width of the Mn-K α calibration line as mentioned before, and the average of the three FI CCDs gives $\sigma_{\text{inst}} = 40 \pm 4 \text{ eV}$. Thus, the measured width is consistent with that expected from the instrumental and intrinsic widths, $(\sigma_{\text{inst}}^2 + \sigma_0^2)^{1/2} = 49 \pm 2 \text{ eV}$, where the intrinsic width σ_0 includes also the thermal Doppler although it is negligibly small ($\sim 2 - 3 \text{ eV}$) in the energy range of interest. The turbulent broadening is then loosely constrained as $\sigma_{\text{turb}} < 32 \text{ eV} \sim 1400 \text{ kms}^{-1}$ (90% confidence). Although σ_0 significantly increases below a temperature of 2 keV, it is within the range of $26 \text{ eV} < \sigma_0 < 30 \text{ eV}$ as long as $2 \text{ keV} < kT < 4 \text{ keV}$, and does not significantly affect the above discussion. The derived limit on σ_{turb} is consistent with a stronger constraint, $< 800 \text{ kms}^{-1}$, derived by an argument that strong turbulence would smear out, via diffusion, the observed abundance gradient in the central 100 kpc of the cluster (Graham et al. 2006).

Observations of resonance scattering of the X-ray emission lines will provide another way to constrain the ICM turbulent motion. This is, however, beyond the scope of the present paper.

5. Summary

Based on Suzaku XIS observations of the Centaurus cluster, we investigated the bulk motion in the intracluster medium to constrain its dynamical state. The high sensitivity and accurate calibration of the XIS sensors enabled us to study positional dependence of the iron-K line energy on a 50 kpc scale, particularly over the central 240 kpc region, as well as on a 140 kpc scale over a di-

ameter of 460 kpc. The results show that there is no significant velocity gradient, within the present calibration uncertainty of $\pm 660 \text{ km s}^{-1}$, suggesting that the bulk velocity does not largely exceed the thermal velocity of the gas. The 90% upper limit on the velocity separation between a pair of regions is $|\Delta v| < 1400 \text{ km s}^{-1}$, providing a tighter constraint than the previous observations by a factor of ~ 2 . The present result cannot be easily reconciled with the previous Chandra observations which reported the large velocity gradients in the two pairs of rectangular regions near the cluster core. The mean redshift of the ICM is determined to be 0.0097, in agreement with the optical redshift of the cluster within the calibrational error. With the upper limit on the velocity difference, the pressure support due to hypothetical rotational motion may not alter the cluster mass estimate under the hydrostatic assumption by more than a factor of ~ 3 .

We are grateful to all the members of the Suzaku Science Working Group, especially T. Tsuru and H. Nakajima for comments on the XIS energy scale, Y. Ishisaki for useful suggestions on the ray-tracing simulations, and N. Y. Yamasaki for discussions. N. O. acknowledges support from the Special Postdoctoral Researchers Program of RIKEN.

References

- Allen, S. W., & Fabian, A. C. 1994, MNRAS, 269, 409
 Churazov, E., Gilfanov, M., Forman, W., & Jones, C. 1999, ApJ, 520, 105
 Dubau, J., & Volonte, S. 1980, Reports of Progress in Physics, 43, 199
 Dupke, R. A., & Bregman, J. N. 2001, ApJ, 562, 266
 Dupke, R. A., & Bregman, J. N. 2005, ApJS, 161, 224
 Dupke, R. A., & Bregman, J. N. 2006, ApJ, 639, 781
 Fabian, A. C., Sanders, J. S., Taylor, G. B., & Allen, S. W. 2005, MNRAS, 360, L20
 Fukazawa, Y., Ohashi, T., Fabian, A. C., Canizares, C. R., Ikebe, Y., Makishima, K., Mushotzky, R. F., & Yamashita, K. 1994, PASJ, 46, L55
 Furusho, T., Yamasaki, N. Y., Ohashi, T. S. R., Kagei, T., Ishisaki, Y., Kikuchi, K., Ezawa, H., & Ikebe, Y. 2001, PASJ, 53, 421
 Graham, J., Fabian, A. C., Sanders, J. S., & Morris, R. G. 2006, MNRAS, 368, 1369
 Hattori, M., Kneib, J., & Makino, N. 1999, Progress of Theoretical Physics Supplement, 133, 1
 Ikebe, Y., Makishima, K., Fukazawa, Y., Tamura, T., Xu, H., Ohashi, T., & Matsushita, K. 1999, ApJ, 525, 58
 Inogamov, N. A., & Sunyaev, R. A. 2003, Astronomy Letters, 29, 791
 Ishisaki, Y., et al. 2006, PASJ, this volume
 Koyama, K., et al. 2006, PASJ, this volume
 Lucey, J. R., Currie, M. J., & Dickens, R. J. 1986, MNRAS, 221, 453
 Makishima, K., et al. 2001, PASJ, 53, 401
 Mitsuda, K., et al. 2006, PASJ, this volume
 Mohr, J. J., Mathiesen, B., & Evrard, A. E. 1999, ApJ, 517, 627
 Norman, M. L., & Bryan, G. L. 1999, LNP Vol. 530: The Radio Galaxy Messier 87, 530, 106
 Ota, N., Pointecouteau, E., Hattori, M., & Mitsuda, K. 2004, ApJ, 601, 120
 Roettiger, K., Burns, J. O., & Loken, C. 1996, ApJ, 473, 651
 Sanders, J. S., & Fabian, A. C. 2002, MNRAS, 331, 273
 Sanders, J. S., & Fabian, A. C. 2006, MNRAS, accepted (astro-ph/0607113)
 Serlemitsos, P., et al. 2006, PASJ, this volume
 Sunyaev, R. A., Norman, M. L., & Bryan, G. L. 2003, Astronomy Letters, 29, 783
 Takahashi, I., Kawaharada, M., Makishima, K., Ikebe, Y., & Tamura, T. 2004, The Riddle of Cooling Flows in Galaxies and Clusters of galaxies, 135
 Takahashi, T., et al. 2006, PASJ, this volume